Journal of Medicinal Chemistry

Article

pubs.acs.org/jmc

# Structure-Based Design of Novel Benzoxazinorifamycins with Potent Binding Affinity to Wild-Type and Rifampin-Resistant Mutant *Mycobacterium tuberculosis* RNA Polymerases

Sumandeep K. Gill,[†,#] Hao Xu,[‡,#] Paul D. Kirchhoff,[§] Tomasz Cierpicki,[∥] Anjanette J. Turbiak,[‡] Baojie Wan,[⊥] Nan Zhang,[⊥] Kuan-Wei Peng,[⊥] Scott G. Franzblau,[⊥] George A. Garcia,[†,‡] and H. D. Hollis Showalter*[,‡,§]

[†]Interdepartmental Program in Chemical Biology, [‡]Department of Medicinal Chemistry, [§]Vahlteich Medicinal Chemistry Core, and [∥]Department of Pathology, University of Michigan, Ann Arbor, Michigan 48109, United States

[⊥]Institute for Tuberculosis Research, College of Pharmacy, University of Illinois at Chicago, Chicago, Illinois 60612-7231, United States

Supporting Information

**ABSTRACT:** By utilization of three-dimensional structure information of rifamycins bound to RNA polymerase (RNAP) and the human pregnane X receptor (hPXR), representative examples (**2b**–**d**) of a novel subclass of benzoxazinorifamycins have been synthesized. Relative to rifalazil (**2a**), these analogues generally display superior affinity toward wild-type and Rif-resistant mutants of the *Mycobacterium tuberculosis* RNAP but lowered antitubercular activity in cell culture under both aerobic and anaerobic conditions. Lowered affinity toward hPXR for some of the analogues is also observed, suggesting a potential for reduced Cyp450 induction activity. Mouse and human microsomal studies of analogue **2b** show it to have excellent metabolic stability. Mouse pharmacokinetics in plasma and lung show accumulation of **2b** but with a half-life suggesting nonoptimal pharmacokinetics. These studies demonstrate proof of principle for this subclass of rifamycins and support further expansion of structure–activity relationships (SARs) toward uncovering analogues with development potential.

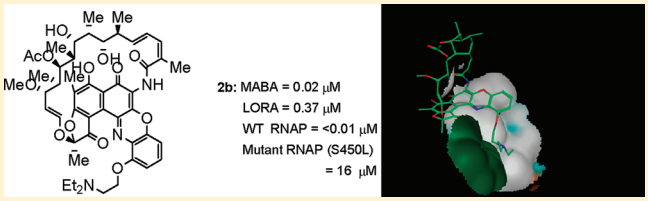


## INTRODUCTION

Tuberculosis (TB) is a contagious and deadly disease that has reached pandemic proportions. According to the World Health Organization (WHO), 8–10 million new cases of TB are diagnosed each year, making *Mycobacterium tuberculosis* (MTB) a leading cause of death in adults (2–3 million/year) due to an infectious agent.[1] A high proportion of these new cases and deaths occur in HIV-positive people with a significant number of AIDS deaths in Africa being attributed to TB infections. Global population growth is increasing the disease burden, posing a continuing health and financial burden in various parts of the world, particularly Asia and Africa.

TB is caused predominantly by MTB, an obligate aerobic bacillus that divides at an extremely slow rate. The chemical composition of its cell wall includes peptidoglycans and complex lipids, in particular mycolic acids, which are a significant determinant of its virulence.[2,3] The unique structure of the cell wall of MTB allows it to lie dormant for many years as a latent infection, particularly as it can grow readily inside macrophages, hiding it from the host's immune system.

The continuing rise in multidrug-resistant strains of MTB (MDR-TB) has further contributed to the dire need for new TB antibiotics, as no new TB drugs have been introduced into clinical use in the past 4 decades.[4,5] Drugs that are active against resistant forms of TB are less potent, more toxic and need to be taken for an extended period of time (≥18 months). The recent emergence of virtually untreatable extensively drug-resistant TB (XDR-TB) poses a new threat to TB control worldwide. Furthermore, effective treatment of TB in persons co-infected with HIV is complicated because of drug–drug interactions. Shorter and simpler regimens that are safe, well tolerated, and effective against drug-susceptible and drug-resistant TB, which are appropriate for joint HIV–TB treatment and amenable to routine clinical settings, are needed urgently.[6,6b]

The rifamycins are the most commonly used drugs for TB, and semisynthetic derivatives have been reported that show improved antimycobacterial activities.[7] These include rifampin (**1a**, RMP, Figure 1), which is the cornerstone of current short-term tuberculosis treatment. Among newer derivatives, rifalazil (**2a**, RLZ, Figure 1) has proved most interesting not just because of its excellent potency but also because of its relative lack of toxicity in early rodent studies.[8] RLZ is an exceedingly potent rifamycin derivative, being 16–256 times more potent than RMP,[9] and is particularly effective against many of the RMP-resistant strains of MTB.[9b,10] Several studies involving strains with various *rpoB* mutations clearly indicated that the

**Received:** December 20, 2011
**Published:** March 27, 2012

ACS Publications © 2012 American Chemical Society

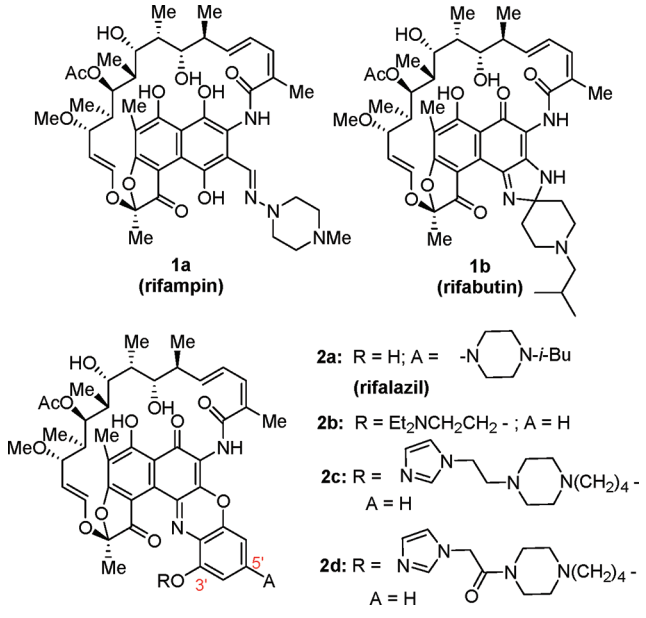


**Figure 1.** Structures of reference agents (**1a**, **1b**, **2a**) and novel benzoxazinorifamycins (**2b–d**).

mutations identified with the RMP, rifapentine, and rifabutin resistant strains retained sensitivity to RLZ.[11] RLZ and its benzoxazinorifamycin analogues also have showed excellent activity against other organisms with RMP-resistant mutations, including *Streptococcus pyogenes*, *Chlamydia trachomatis*, and *Chlamydia pneumonia*.[12]

In mouse in vivo efficacy studies, RLZ has been shown to be clearly more potent than RMP including activity against some RMP-resistant strains,[9a,c,13,14] and longer term MTB studies in combination with other agents indicated that the same level of cure could be achieved with shorter (at least 2-fold) duration of treatment with RLZ compared to RMP.[15] In pharmacokinetic (PK) studies, RLZ has shown a high volume of distribution and produced tissue levels in rats up to 200 times those in plasma. It displayed a very long half-life (60–100 h) in human trials.[16]

One major downside to the rifamycins used to treat TB is their many drug–drug interactions. This effect appears to be diminished with RLZ, as shown in rat and the dog studies.[17] This study also showed RLZ not to be an inducer of hepatic cytochrome P450 (Cyp450). In a series of phase I[18,19] and phase II[9a,18−20] clinical trials, RLZ proved to be quite toxic, with most adverse effects associated with a flulike syndrome and leucopenia even at lower dose levels. Hence, its development for TB indications has been suspended.[21]

In this paper, we detail the structure-based design, synthesis, and biological evaluation of representative compounds (**2b–d**, Figure 1) of a novel subclass of RLZ (**2a**) in which ether tethers have been installed off the 3′-position of the "southeastern" part of the benzoxazinorifamycin template. Our expectation was that this modification would provide analogues with equal or better potency than RLZ against wild-type and Rif-resistant (RifR) mutants of RNA polymerase (RNAP), the molecular target of the rifamycins, while retaining good antitubercular activity in vitro. We also expected our compounds to display lowered binding toward activation of the human pregnane X receptor (hPXR).

## RESULTS AND DISCUSSION

**Analogue Design.** Our impetus to investigate the RLZ subclass, exemplified by analogues **2b–d**, was driven by its ease of synthesis and the likelihood that compounds with lowered or absent Cyp450 induction effects would be generated. This latter expectation was based on the known diminution of Cyp450 induction with the progression from RMP (**1a**, hydroquinone core) to rifabutin (**1b**, RFB, modified quinone core) to RLZ (**2a**, markedly modified quinone core) subtypes. Within this same order of structural subclasses, there also is a trend of RLZ possessing increased potency against drug-susceptible isolates of slow-growing mycobacteria and better in vivo efficacy in mice.[9c]

Recent determinations of the three-dimensional structures of rifamycins bound to RNAP now provide a conceptual framework for structure-based discovery of improved rifamycins. Our analysis of the recently published structures has revealed an approach for the chemical elaboration of the ansanapthalene core in a novel way that should lead to enhanced binding affinity to both wild-type and resistant mutants. Analysis of a recent structure of RMP (**1a**) bound to the human pregnane X receptor (hPXR) suggests that these elaborations may have the significant added benefit of reducing the affinity of the analogues for hPXR, thereby reducing Cyp450 induction activity.

Our modeling was based on the 2.5 Å resolution structure of rifabutin (**1b**) in complex with the *Thermus thermophilus* RNAP holoenzyme (PDB code 2a68).[22] The rifamycin binding site is highly conserved among bacteria; therefore, this structure provides a good foundation for understanding how proposed rifamycin analogues may interact with the MTB RNA polymerase. The crystal structure (2a68) contains two complete complexes. On the basis of observed differences between these two complexes and what is seen in the related complexes present in PDB code 2a69 (rifapentine in complex with the *T. thermophilus* RNAP holoenzyme), these studies suggested that, at least in the free holoenzyme, the $\sigma$ factor hairpin loop may exist in two distinct physiologically relevant conformations.

Although relatively qualitative in nature, our modeling studies suggested a number of analogues with a range of size, flexibility, and spatial variation for interactions with the $\sigma$ hairpin loop and other portions of the RNAP complex. These analogues were chosen with the goal of increasing potency by one or more of the following: (a) making additional contacts with the $\sigma$ factor and $\beta$ and/or $\beta'$ region of the RNAP and (b) interfering with the binding of the $\sigma$ factor and/or further occluding the channel.

Figure 2 displays the modeled RLZ/RNAP complex without bound water molecules. RLZ (**2a**) is shown with bright green carbon atoms. The RNAP molecular surface is shown with the $\beta$ surface colored white and light blue, $\beta'$ in brown, and the $\sigma$ factor in dark green. Figure 3 displays the interaction surfaces at 4.5 Å between the compound tail and surrounding RNAP for benzoxazinorifamycin analogue **2b**, utilizing the same coloring scheme as Figure 2 (similar poses for RLZ, and analogues **2c,d** are shown in Figure 1a–cSI in Supporting Information). These illustrate that the benzoxazinorifamycins have the potential to interact with different regions of RNAP. While the modeling used to produce these poses is qualitative in nature because of the sizes of the channel and the analogues, it shows that the


dx.doi.org/10.1021/jm201716n | J. Med. Chem. 2012, 55, 3814–3826

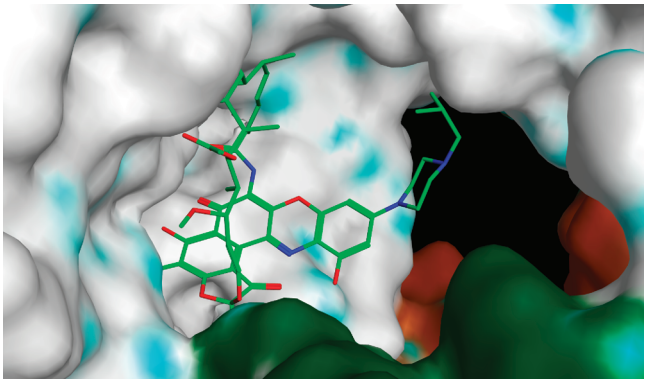

**Figure 2.** Modeled RLZ/RNAP complex without bound water molecules. RLZ (**2a**) is shown with bright green carbon atoms. The RNAP molecular surface is shown with $\beta$ colored white and light blue, $\beta'$ in brown, and the $\sigma$ factor in dark green.

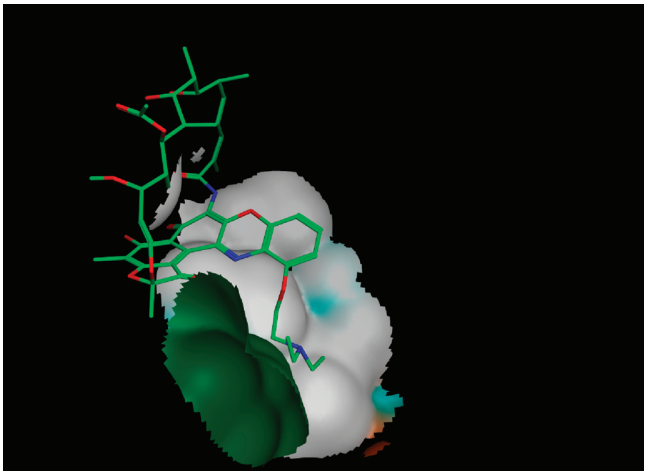

**Figure 3.** Interaction surfaces at 4.5 Å between the compound tail and surrounding RNAP for benzoxazinorifamycin **2b**, in the same coloring scheme as Figure 2.

analogues can pick up additional contacts, which would be expected to translate to different potency profiles.

As noted above, Cyp450 induction effects (due to activation of the hPXR) decrease with a progression from the RMP to the RLZ scaffold. A recent review discusses developments to predict and attenuate enzyme induction and drug–drug interactions that are mediated via activation of hPXR.[23] Much work has been done to develop computational algorithms to predict hPXR activation. However, the most exciting developments have been the determination of a number of X-ray crystal structures of activators bound to the ligand-binding domain of hPXR. Particularly important for our work, the structure of RMP bound to hPXR has been determined.[24]

RMP (**1a**) is one of the, if not the most, potent activators of hPXR.[24] RMP fills the ligand-binding pocket very well, and differences in RMP activation of human versus mouse PXR have been interpreted in light of structural information. For example, Leu308 in the human PXR is replaced by Phe in the mouse, and Ser247 by Trp, leading to the suggestion that these changes impair the binding of RMP to mouse PXR, accounting for the differential RMP activation of these PXRs. The relative potency of CYP3A4 induction is RMP > rifapentine > RFB > RLZ. Figure 4 displays the modeled hPXR binding site with these four rifamycins in spatial relation to resolved hPXR residues (see Experimental Section for details of modeling). In particular, there are seven hPXR residues, namely, Phe237, Ser238, Leu239, Leu240, Pro241, His242, and Met243, very close to the synthetic branch point for our synthesized analogues. These residues are resolved in each of the five hPXR structures and, other than one of the Phe237 rings, have fairly conserved relative coordinates. This, along with the presence of Pro241, would suggest a more rigid region of the hPXR ligand-binding pocket.

The hPXR ligand-binding pocket is large, flexible, and capable of adapting itself to bind a large variety of ligands. What our modeling suggested is that our benzoxazinorifamycin analogues, which are designed to target RNAP $\sigma$ factors, may have the added benefit of overwhelming the normally promiscuous hPXR binding pocket. It appears that the tails of these analogues may prevent binding to hPXR by projecting into rigid, sterically encumbered regions of hPXR. Diminished binding to hPXR would then presumably reduce induction of CYP450s.

**Chemistry.** The synthetic route utilized to make our target "one-armed" compounds **2b–d** is shown in Scheme 1. The RLZ literature[25] suggested a strategy of annulating the benzoxazino moiety onto rifamycin S (**12**) with a suitably protected monoether (e.g., TBS) of 2-aminoresorcinol, followed by ether deprotection and then side chain installation off the nascent phenol by any number of alkylation methodologies. This was investigated, but yields were very poor and the scope of alkylation possibilities was quite limited (data not shown). We opted instead to annulate a fully tethered 2-aminoresorcinol monoether onto the rifamycin S framework in

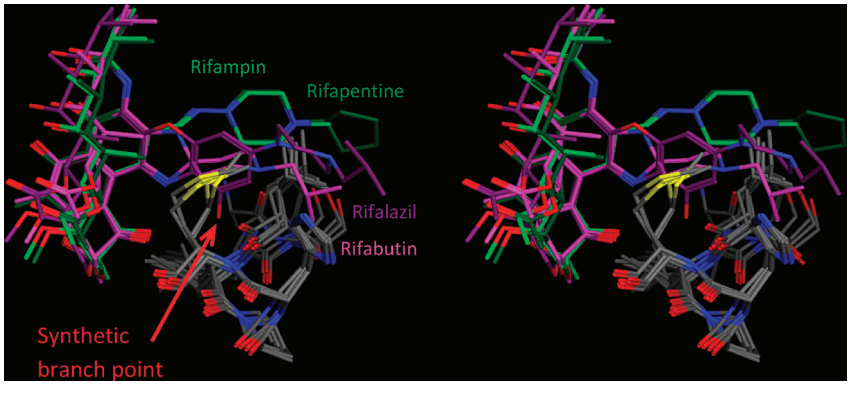


**Figure 4.** Stereoview of clinical rifamycins modeled into the hPXR binding pocket.


dx.doi.org/10.1021/jm201716n | J. Med. Chem. 2012, 55, 3814–3826

**Scheme 1. Synthesis of 2b−d**[a]

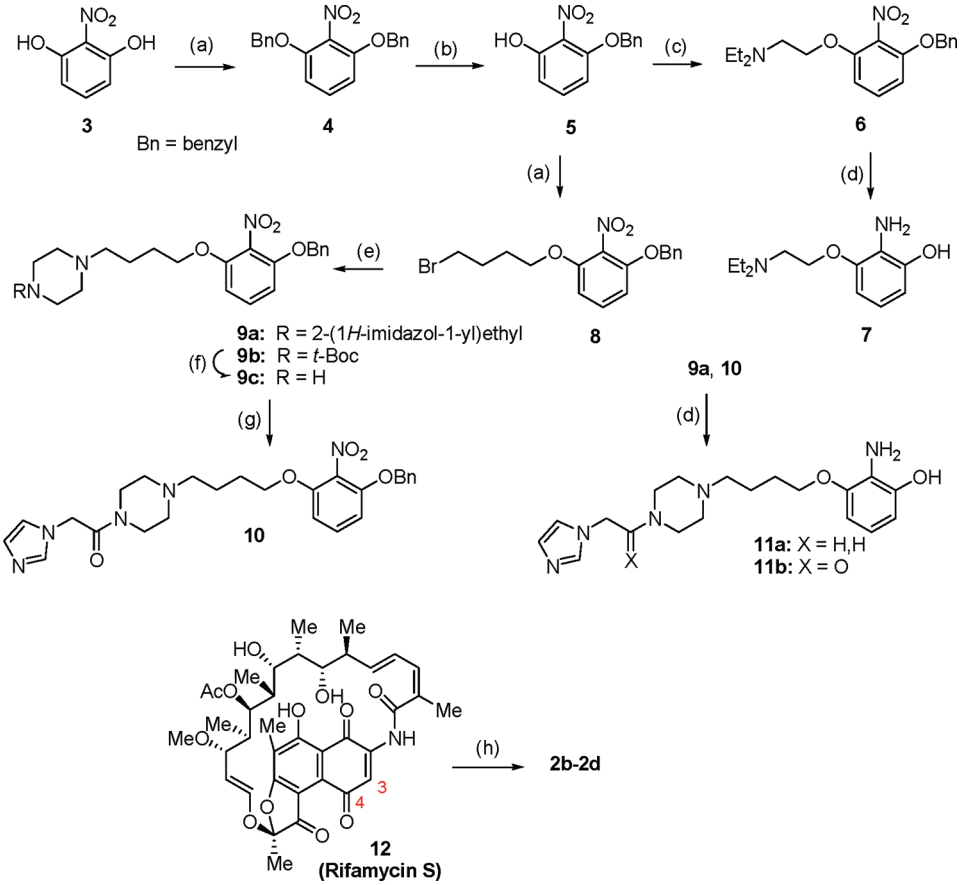


[a]Reagents and conditions: (a) benzyl bromide (for **3**) and 1,4-dibromobutane (for **5**), $Cs_2CO_3$, DMF, 25 °C, 12−16 h, 93−95%; (b) $BCl_3$, DCM, −78 °C, 1 h, 82%; (c) $Et_2NCH_2CH_2Cl$·HCl, $Cs_2CO_3$, acetone, 50 °C, 3 h, 93%; (d) 20% Pd/C, $H_2$ (40 psi), 25 °C, 20−40 h, MeOH/HOAc (9:1) for **6**; MeOH/10% aqueous HCl (9:1) for **9a**, **10**; 81 − 98%; (e) 1-[2-(1*H*-imidazol-1-yl)ethyl]piperazine or 1-Boc-piperazine, DIPEA, $CH_3CN$, reflux, 12−18 h, 68−99%; (f) TFA, DCM, 25 °C, 3 h; (g) 2-(1*H*-imidazol-1-yl)acetic acid, DIPEA, EDC·HCl, HOBT, DMF, 25 °C, 16 h, 72% from **9b**; (h) **7**, **11a**, or **11b**; *p*-dioxane or 1,2-DCE, $MnO_2$, 25 °C to reflux, 35−74%.

a single step. This allowed us to consider a wide range of tethers off the "southeastern" part of the rifalazil-type template and, more importantly, minimized difficult synthetic transformations and product purifications involving the complex rifamycin S core to a single last step. Thus, we set our sights initially on developing a robust procedure to intermediate **5**, which would serve as a key starting material for introduction of our chosen tethers. While there are two reports for the synthesis of this compound,[26,27] neither was deemed practical for our needs. Instead, we pursued a two-step procedure. Accordingly, dialkylation of 2-nitroresorcinol (**3**), similar to the literature procedure,[28] gave a 95% yield of dibenzyl ether **4** which was then cleanly monodebenzylated to nitrophenol **5**[26] in 82% yield. With **5** now in hand, we were ready to install our target tethers. Phenolic alkylation with 2-(diethylaminoethyl)-ethyl chloride hydrochloride under standard conditions provided **6** in 87% yield. Hydrogenation of **6** utilizing Pearlman's catalyst simultaneously reduced the nitro function and hydrogenolyzed the benzyl protecting group to give the 2-aminoresorcinol ether **7** in 81% yield. A similar sequence of reactions was followed to provide ethers **11a**,**b**. Alkylation of **5** with 1,4-dibromobutane gave **8** in 93% yield, which was subsequently aminated with two monosubstituted piperazines to afford compounds **9a** and **9b** in 68% and 99% yields, respectively. *t*-Boc deprotection of **9b** followed by acylation of **9c** with 2-(1*H*-imidazol-1-yl)acetic acid provided **10**, the amide congener of **9a**, in 72% yield. Hydrogenation of **9a** and **10** was conducted as described for **6** to provide the remaining 2-aminoresorcinol ethers **11a** and **11b**, respectively, in nearly quantitative yields. The structure of each 2-aminoresorcinol ether (**7**, **11a**, **11b**) is supported by mass spectrometry along with $^1H$ and $^{13}C$ NMR spectra (Supporting Information, Figure 2SI). Each was then annulated onto rifamycin S (**12**) to provide target compounds **2b−d** in 35−74% yields following a two-stage purification utilizing medium pressure and then preparative plate silica gel chromatography. No effort was made to optimize the condensation reaction with rifamycin S, but we feel that this has the potential to be an efficient transformation.

The structures of **2b−d** were verified by the NMR spectra (Supporting Information, Figure 3SI) and by chemical ionization (CI) and high resolution (HR) mass spectrometry (Supporting Information, Figure 4SI). We found that peaks in 1D NMR spectra of **2b−d** showed significant broadening, which was dependent on the solvent utilized. The spectra in $CDCl_3$ were of higher quality and were selected for the assignment of chemical shifts. For each compound (**2b−d**), we obtained complete and unambiguous assignment for the side chain protons and carbons, verifying their point of attachment onto the benzoxazinorifamycin core as shown (Supporting


dx.doi.org/10.1021/jm201716n | *J. Med. Chem.* 2012, 55, 3814−3826

Information, Tables 1SI and 2SI). In addition, nearly complete assignments were made for rifamycin core proton and carbon atoms. Lack of complete assignment is due to the absence of several peaks as a result of broadening observed in the NMR spectra. The rifamycin core has restricted conformation and the broadening of NMR signals most likely reflects a conformational exchange process, which is further supported by sharpening of the NMR signals upon increasing the sample temperature. Our NMR work provides a significant contribution to the study of rifalazil-type compounds, as there is only one prior report in the literature in which proton and carbon peak assignments have been made.[29]

**In Vitro Inhibition of Wild-Type and RMP-Resistant Mutant MTB RNAPs.** The inhibition constants ($IC_{50}$) of the wild-type and three Rif-resistant (RifR) mutants of the MTB RNAP by RLZ (**2a**) and our analogues (**2b–d**) were determined via dose–response studies as previously described, with each compound tested in duplicate at the specified concentrations.[30] The data were plotted (log of the benzoxazinorifamycin concentration vs % activity) and then fitted by nonlinear regression. The log($IC_{50}$) and their standard errors (of the fit) are reported, with these roughly translating into a 20–25% error in the $IC_{50}$ values (Supporting Information, Table 3SI). The apparent $IC_{50}$ values are listed in Table 1. Not surprisingly, all of the benzoxazinorifamycins (**2a–d**) inhibit the wild-type MTB RNAP in the $10^{-9}$ M (nM) range. We note that the lower limit of detection of this assay is $IC_{50} \approx 5$ nM. It is quite possible that these compounds have true $IC_{50}$ values much lower than this. A more sensitive assay to determine these very low $IC_{50}$ values is currently being developed in our lab. The $IC_{50}$ values for RLZ (**2a**) against the RifR mutants of MTB were much higher, in the $10^{-4}$ M (~100 $\mu$M) range. The most frequently observed MTB RifR mutant in clinical isolates, S450L,[31] was inhibited at ~7-fold lower concentration of **2b** and **2c** relative to RLZ with **2d** being essentially the same as RLZ. The MTB D435V mutant was inhibited at 26- to 60-fold lower concentrations of **2b–d** relative to RLZ. Interestingly, the H445Y mutant appears to retain resistance to all tested benzoxazinorifamycins. The results within this very limited series of our designed analogues provide proof of principle that the potency of rifamycins toward RifR MTB RNAPs can be substantially improved.

**Table 1. In Vitro RNAP $IC_{50}$ Values ($\mu$M)[a] for RLZ (2a) and Analogues (2b–d)**

| | 2a (RLZ) | 2b | 2c | 2d |
|---|---|---|---|---|
| WT RNAP ($-\sigma^A$) | 0.0115 | <0.01 | <0.01 | <0.01 |
| WT RNAP ($+\sigma^A$) | <0.01 | <0.01 | <0.01 | <0.01 |
| D435 V ($+\sigma^A$) | 541 | 20 | 9 | 13 |
| H445Y ($+\sigma^A$) | 172 | 171 | 437 | 574 |
| S450L ($+\sigma^A$) | 117 | 16 | 18 | 122 |

[a] $IC_{50}$ is the concentration of rifamycin resulting in 50% inhibition of transcription. Errors of the log($IC_{50}$) values are reported as described in the Experimental Section. As a control, the mutant RNAPs (D435 V, H445Y, and S450L) without SigA were tested against RMP where the $IC_{50}$ values are as follows: 313 $\mu$M (D435 V), 830 $\mu$M (H445Y), and 126 $\mu$M (S450L).

**Activity against *M. tuberculosis* ($H_{37}R_V$) in Cell Culture.** The compounds were screened in assays to quantify their antitubercular activity under both aerobic and anaerobic conditions (Table 2). Briefly, the 8-day microplate-based assay using Alamar Blue reagent (added on day 7) for determination of growth (MABA)[32] gives an assessment of activity against replicating MTB, while the 11-day high-throughput, luminescence-based low-oxygen-recovery assay (LORA)[33] measures activity against bacteria in a nonreplicating state that models clinical persistence. Minimum inhibitory concentration ($MIC_{90}$) is defined as the lowest compound concentration effecting >90% growth inhibition.

**Table 2. $MIC_{90}$ Values ($\mu$M)[a] of RMP (1a) and Benzoxazinorifamycins 2a–d vs MTB**

| | 1a (RMP) | 2a (RLZ) | 2b | 2c | 2d |
|---|---|---|---|---|---|
| MABA | 0.13 | <0.004 | 0.02 | 0.08 | 0.07 |
| LORA | 0.46 | <0.017 | 0.37 | 0.35 | 0.40 |

[a] The $MIC_{90}$ is defined as the minimum concentration of the compound required to inhibit 90% of bacterial growth: isoniazid (MABA, 0.24; LORA, >128); moxifloxacin (MABA, 0.46); streptomycin (MABA, 0.46); PA824 (LORA, 2.53).

Under aerobic conditions (MABA), all newly synthesized compounds **2b–d** display superior activities ($MIC_{90}$ of 0.02–0.08 $\mu$M) relative to RMP (**1a**, 0.13 $\mu$M) but are less potent (5- to 40-fold) than RLZ (**2a**, <0.004 $\mu$M). Under anaerobic conditions (LORA), activity for compounds **2b–d** ($MIC_{90}$ of 0.35–0.40 $\mu$M) is essentially equivalent to that for RMP, and these range from 4- to 18.5-fold higher than in the MABA. Relative to RLZ, LORA potency for analogues **2b–d** is lower (at least 20-fold).

**Activation of hPXR.** As discussed above, one of the limiting factors for rifamycin utility in humans is their extremely high potency toward activation of the human pregnane X receptor (hPXR). To probe this, we have used a commercial in vitro assay for hPXR activation (Puracyp, Inc.). Figure 5 shows dose–response plots for this assay. RMP, as previously known, exhibits a high maximal degree of activation (~12-fold) and an $EC_{50}$ of ~2 $\mu$M. RLZ has been reported to have essentially no ability to activate hPXR. Our data confirm that at concentrations lower than 100 $\mu$M, RLZ exhibits no detectable activation of hPXR. At 100 $\mu$M, RLZ does show ~2-fold activation; however, it also shows ~2-fold loss of cell viability (suggesting cytotoxicity) at this concentration.

Analogue **2d** was fit to a dose–response curve (Figure 5) that revealed a 6-fold maximal activation of hPXR and an $EC_{50}$ of ~6 $\mu$M, both parameters within 2- to 3-fold of those for RMP. This analogue also starts to exhibit loss of cell viability at 25 $\mu$M (Table 4SI in Supporting Information and Figure 6) such that the 100 $\mu$M data point was not used in the dose–response curve fit, again similar to RMP. Analogues **2b** and **2c** were essentially identical with ~3-fold hPXR activation at 6.25 $\mu$M and dramatic loss of cell viability above 6.25 $\mu$M masking any further hPXR activation, as seen in Figure 5.

Our modeling suggests that the additional bulk of our analogues should reduce binding to hPXR due to steric clashes within the binding pocket. It seems likely that the flexible side chains may allow for the side chains to adopt a conformation that minimizes this clash. We have no explanation for the apparent toxicities (in this cell line under the conditions of the hPXR activation assay) of **2b** and **2c**. Further studies in this and other cell lines are needed to confirm this toxicity and to probe the associated mechanism. At least for the wild-type RNAP, there is ~1000-fold difference between the RNAP $IC_{50}$ and the threshold for apparent cytotoxicity.

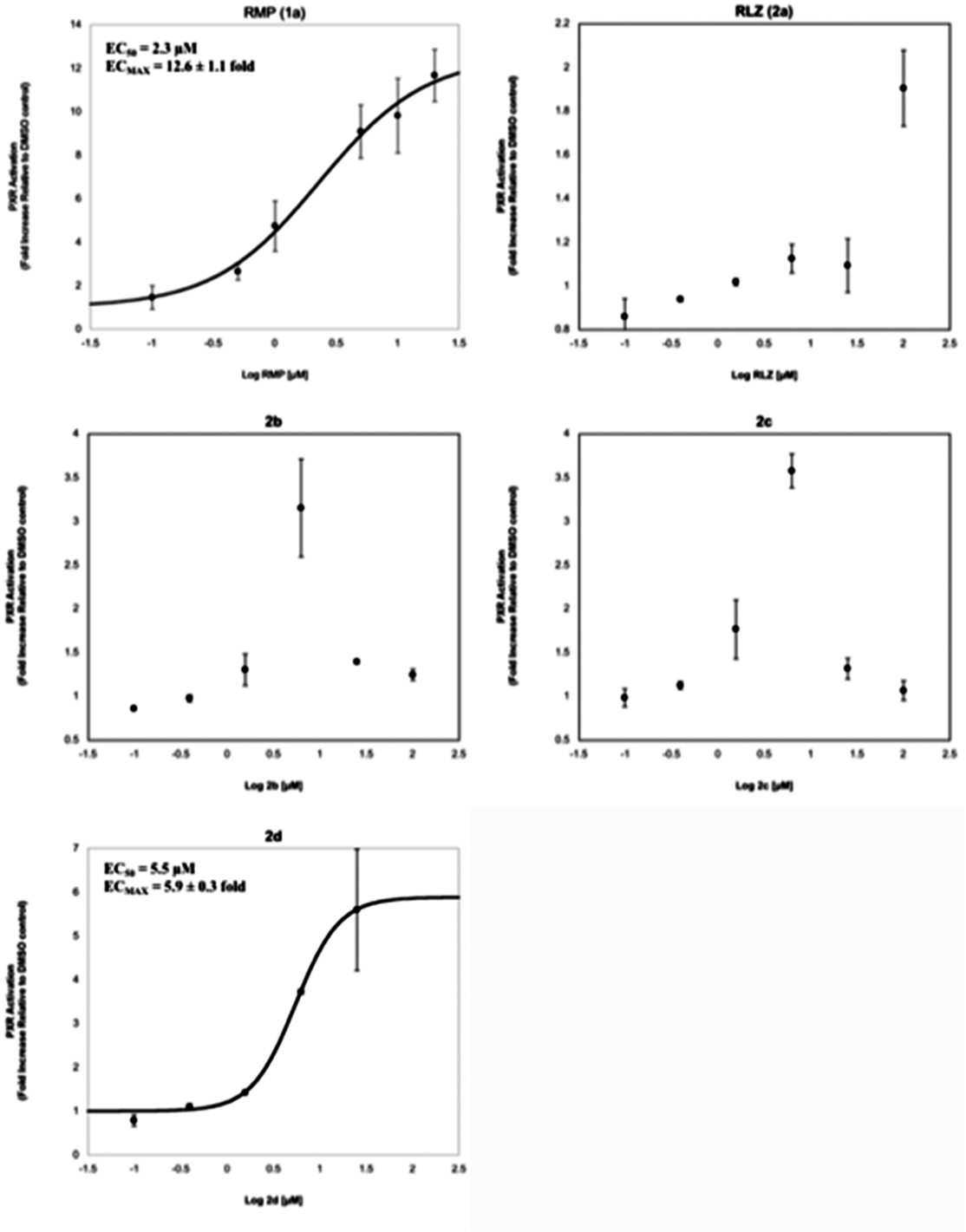


**Figure 5.** Plots from human pregnane X receptor (hPXR) activation assay.

**Microsome Stability and Pharmacokinetics.** RLZ (**2a**) and analogue **2b** were evaluated for metabolic stability in human microsomes. Each is relatively stable with estimated half-lives of 65 and 54 min, respectively (Table 3). Similarly, the estimated half-life of **2a** in mouse microsomes is 53 min while that of **2b** is 141 min.

The PK of analogue **2b** was assessed using a suspension prepared in carboxymethylcellulose (0.05% CMC). In the single dose study, **2b** was detected in the blood but the signal was below the lower limit of quantitation. The $C_{max}$ was 0.0185 $\mu$M at a $T_{max}$ of 1 h. However, analogue **2b** appears to accumulate in the blood of mice that were dosed once daily for 5 consecutive days with a $C_{max}$ of 1.74 $\mu$M at a $T_{max}$ of 2 h, which is 100-fold higher than that observed after a single oral dose (Supporting Information, Figure 6SI). In the lung tissue of these mice, **2b** was also detected at 1.79 $\mu$g/g (around 0.4 $\mu$M) but only exceeded the MIC of 0.02 $\mu$M for ~4 h (Supporting Information, Figure 7SI).

## CONCLUSIONS

We have utilized recent determinations of the three-dimensional structures of rifamycins bound to RNAP to design and synthesize representative examples (**2b–d**) of a novel subclass of benzoxazinorifamycins possessing a range of size, flexibility,


dx.doi.org/10.1021/jm201716n | J. Med. Chem. 2012, 55, 3814–3826

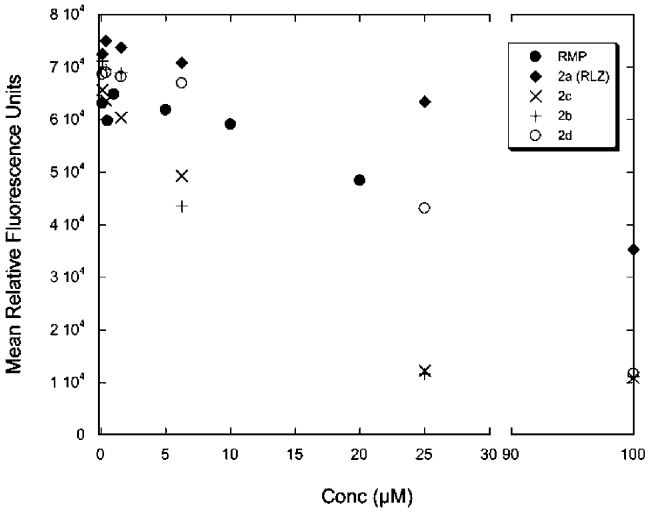


**Figure 6.** Effect of rifamycins on DXP2 cell growth as measured by CellTiter-Fluor.

**Table 3. Half-Life of Selected Benzoxazinorifamycins in Human and Mouse Microsomes**

| | % remaining compd after 30 min of incubation in microsomes | | $t_{1/2}$ (min) | |
|---|---|---|---|---|
| compd | mouse | human | mouse | human |
| **2a** (RLZ) | 67 | 73 | 53 | 65 |
| **2b** | 86 | 68 | 141 | 54 |

and spatial variation to interact with the $\sigma$ hairpin loop and other regions of the RNAP complex. Relative to RLZ (**2a**), these analogues generally display superior affinity toward wild-type and Rif-resistant mutants of the MTB RNAP but lowered antitubercular activity in cell culture under both aerobic and anaerobic conditions. The lowered activity in cell culture may be due to poorer permeability and is under investigation. We have also utilized information from the crystal structure of RMP (**1a**) bound to hPXR as part of our design strategy toward analogues **2b–d**. Unfortunately, these analogues exhibit both hPXR activation and cytotoxicity at a concentration above 25 $\mu$M.

Mouse and human microsomal studies of analogue **2b** show it to have excellent metabolic stability relative to RLZ (**2a**). The pharmacokinetics of **2b** showed accumulation of the compound in plasma after multiple dosing with an apparent half-life of ~1–2 h, suggesting that compound levels are above the MIC for ~7–8 h if the decay is linear. This is corroborated by studies in lung tissue where levels of **2b** exceeded the MIC of 0.02 $\mu$M for only ~4 h. These studies suggest nonoptimal pharmacokinetics for this compound and that further SAR will be necessary to find a compound to take to in vivo efficacy studies.

Apart from an obscure report on the synthesis of a small series of simple benzoxazinorifamycin C-3′ monoethers,[34] there are no examples of more elaborate ethers that have been incorporated onto a rifamycin S scaffold utilizing the strategy we outline. Furthermore, our work is the first example that we are aware of where structure-based design has been utilized to target binding to specific $\sigma$ factors within the complex RNA polymerase machinery. Our synthetic strategy of annulating a fully tethered 2-aminoresorcinol monoether onto the rifamycin S framework in a single step is efficient and allows for a wide range of tethers off the 3′-position of the rifalazil-type template, which augurs well for a rapid expansion of the SAR within this novel subclass.

## EXPERIMENTAL SECTION

**Computational Modeling of Rifamycin–RNAP Complexes.** The structure of 2a68 was used as the starting point in our modeling studies. In brief, modifications made to the structure prior to its use in the modeling were as follows: All water molecules and metals greater than 12 Å from rifabutin (**1b**, RFB) were removed. Four magnesium ions within 12 Å were converted to water molecules. Partially missing residues were repaired. Connection points for completely missing residues were greater than 35 Å from RFB and were kept fixed in space during the energy minimizations. All N and C termini, either real or as a result of missing residues, were acetylated and amidated, respectively. RFB was removed from the complex. Hydrogen atoms were added to the proteins, and the force field was set to AMBER99 and charged.

A series of energy minimizations were then conducted to relax the positions of the modified atoms using the AMBER99 force field to gradients of 0.01. Positions of hydrogen atoms were first relaxed with energy minimization. Repaired residues except for their C$\alpha$ atoms, termini, and hydrogen atoms were then relaxed. Lastly, the complete repaired residues, termini, and hydrogen atoms were relaxed. Resulting confirmations of the repaired residues and termini were checked. Bond orders for RFB were corrected. Hydrogen atoms were added, and the force field was set to MMFF94x and charged. Positions of hydrogen atoms were relaxed with energy minimization using the MMFF94x force field to a gradient of 0.01. RFB was returned to the complex in its original pose.

A second series of energy minimizations were then conducted using the MMFF94x force field to gradients of 0.01. Positions of hydrogen atoms were first relaxed followed by positions of hydrogen atoms and all water molecules. Atoms of the RFB were then included in the minimizations. Lastly, positions of all RFB, water, and hydrogen atoms and protein residues having one or more atoms within 12 Å from RFB were relaxed with energy minimization. The naphthalene ring of RFB drifted approximately 1 Å toward the cleft of the complex from their crystallographic positions with relatively minor movements of the protein residues well within the 2.5 Å resolution of the starting structure.

Complexes for proposed analogues were generated from the modified RFB complex in the following way: All water molecules present in the structure were removed. All residues not having one or more atoms within approximately 20 Å of the RFB were deleted. The RFB structure was modified to generate the proposed analogue. Atoms of the RFB, which were not modified in the generation of the proposed analogue, were initially fixed in space and treated as part of the RNAP holoenzyme. Modifications were made to the RFB structure to produce the proposed analogue while keeping the unmodified atoms of RFB fixed in relation to the RNAP complex. A LowModeMD[35] conformational search algorithm with energy minimization was then employed to generate plausible poses (conformations) of the modified portions of RFB. The LowModeMD search was conducted in MOE[36] using default settings. Hydrogen atoms, modified portions of RFB, and protein side chains within ~16 Å of the modified portions were allowed to move during the conformational search and energy minimizations. Generated poses were ranked by interaction energies and duplicate poses based on a rmsd cutoff removed.

The lowest energy pose was then selected and the truncated RNAP complex soaked with water to a surrounding distance of 6 Å. As described above, a series of energy minimizations were then conducted using the MMFF94x force field to relax the complex. First, hydrogen atoms and then the water molecules were allowed to relax while the entire analogue and all of the RNAP atoms were held fixed. Second, the modified portions of RFB and side chains of RNAP within 16 Å were also allowed to relax with the water molecules and hydrogen atoms. Finally, the entire analogue molecule, residues of RNAP within

16 Å, and the water molecules and hydrogen atoms were allowed to relax. The relaxed complexes were then examined to determine how the proposed analogue may interact with the $\sigma$ factor or other portions of RNAP (specifically the $\beta$ and $\beta'$ subunits).

**Computational Modeling of Rifamycin−hPXR Complexes.** The 3D structures in Figure 4 were generated using the 2.5 Å resolution crystal structure for *Thermus thermophilus* RNAP in complex with rifabutin (**1b**, RFB) obtained from the Protein Data Bank (PDB code 2a68).[22] As described above, coordinates for RFB were relaxed in the presence of the RNAP using a series of energy minimizations with decreasing constraints on the surrounding protein atoms, and water molecules. Coordinates for RMP, rifapentine, and RLZ were created and relaxed in the same fashion after modifying RFB. A 2.8 Å resolution crystal structure of hPXR in complex with rifampin is available from the Protein Data Bank (PDB code 1skx).[24] Unfortunately, the 1-amino-4-methylpiperazine tail of RMP and three hPXR loops adjacent to the binding pocket (residues 178−209, 229−235, and 310−317) are disordered and unresolved in the structure. The missing residues in this and other published hPXR structures make accurate modeling of the hPXR and the tails of rifamycins difficult. Figure 4 was created by overlaying the naphthalene portions of the four rifamycins generated from the 2a68 structure onto the naphthalene portion of RMP in complex with hPXR structure 1skx. The relative location of synthetic branch point for the analogues described in Figure 1 is also indicated in Figure 4. In addition to the complex with RMP, four other relatively complete hPXR structures are available. The hPXR apo structure (PDB code 1ilg)[37] and hPXR complexes with SR12813 (PDB code 1ilh),[37] hyperforin (PDB code 1m13),[38] and colupulone (PDB code 2qnv)[39] were obtained from the Protein Data Bank. These four hPXR complexes were superimposed onto the hPXR structure of 1skx containing the four modeled in rifamycins. Coordinates were not relaxed with energy minimization because of the many missing residues.

**Chemistry.** *Materials and Methods.* All reagents were commercially available and used without further purification. Rifalazil (**2a**, RLZ) of 98.3% purity by HPLC was synthesized and purified as previously described.[25] Melting points were determined in open capillary tubes on a Laboratory Devices Mel-Temp apparatus and are uncorrected. Routine $^1$H and $^{13}$C NMR spectra were obtained on a Bruker 500 MHz spectrometer with $CDCl_3$, $CD_3OD$, or DMSO-$d_6$ as solvent, and chemical shifts are reported relative to the residual solvent peak in $\delta$ (ppm). For compounds **2b−d**, 1D NMR spectra were investigated in different solvents including $CDCl_3$, DMSO-$d_6$, and pyridine-$d_5$, with $CDCl_3$ yielding spectra of highest quality. The $^1$H, $^{13}$C, $^1$H−$^{13}$C HSQC and COSY experiments were measured at 25 °C using a 600 MHz Bruker spectrometer equipped with a cryogenic probe. Use of a cryogenic probe resulted in some distortion of the $^{13}$C baseline due to the high *Q*-value of the probe (see Supporting Information, Figure 3SI); however, this did not affect the analysis of the spectra. Mass spectrometry analysis was performed using a Waters LCT time-of-flight mass spectrometry instrument. High resolution mass spectrometry (HRMS) analysis was performed on an Agilent Q-TOF system. Compound purity for target benzoxazinorifamycins **2b−d** was assessed by analytical HPLC, which was performed on a Agilent 1100 series system with an Agilent Eclipse plus C18 (4.6 mm × 7.5 mm, 3.5 mm particle size) column. The mobile phase was a 11 min binary gradient of acetonitrile (containing 0.1% TFA) and water (10−90%). HPLC traces of benzoxazinorifamycins **2b−d** are shown in Supporting Information, Figure 5SI. Thin-layer chromatography (TLC) was performed on silica gel GHLF plates (250 $\mu$m) purchased from Analtech. Extraction solutions were dried over $MgSO_4$ prior to concentration.

*(((2-Nitro-1,3-phenylene)bis(oxy))bis(methylene))dibenzene (**4**).* A mixture of 2-nitroresorcinol (**3**, 2.0 g, 12.9 mmol), $Cs_2CO_3$ (10.5 g, 32.2 mmol), benzyl bromide (3.39 mL, 28.4 mmol), and DMF (35 mL) was stirred at room temperature for 12 h. The mixture was diluted with ethyl acetate and washed sequentially with 1% aqueous HCl and brine. The organic phase was dried and concentrated to leave a yellow oil, which was diluted with 2-propanol to precipitate pure product. The solids were collected to leave **4** (4.11 g, 95%) as light yellow crystals: mp 87.5−88 °C (lit.[28] 80 °C); $R_f$ = 0.26 (hexanes/ethyl acetate, 5:1); $^1$H NMR ($CDCl_3$) $\delta$ 7.3 (m, 10 H), 7.23 (t, $J$ = 8.5 Hz, 1 H), 6.64 (d, $J$ = 8.5, 2 H), 5.16 (s, 4 H); $^{13}$C NMR ($CDCl_3$) $\delta$ 150.9, 135.6, 130.9, 128.7, 128.2, 127.0, 106.2, 71.0; MS (ES$^+$) $m/z$ 358.1 (M + Na)$^+$.

*3-(Benzyloxy)-2-nitrophenol (**5**).* A solution of dibenzyl ether **4** (3.0 g, 8.95 mmol) in dichloromethane (80 mL) at −78 °C was treated dropwise with boron trichloride (13 mL, 1 M in heptane) during which the color changed to dark purple. The reaction was monitored by TLC, and the mixture was stirred at −78 °C until all starting material was consumed (1 h). Methanol (5 mL) was added dropwise, and the mixture was brought to room temperature, diluted with water, and then extracted with dichloromethane (2×). The combined extracts were dried and concentrated to an orange oil that was purified by flash silica gel chromatography, eluting with hexanes/ethyl acetate (5:1). Product fractions were pooled and concentrated to give **5** (1.79 g, 82%) as a bright yellow solid: mp 67−67.5 °C; $R_f$ = 0.24 (hexanes/ethyl acetate, 5:1); $^1$H NMR ($CDCl_3$) $\delta$ 10.18 (brs, 1 H), 7.4 (m, 2 H), 7.3 (m, 4 H), 6.72 (d, $J$ = 8.5 Hz, 2 H), 6.6 (d, $J$ = 8.5 Hz, 2 H), 5.21 (s, 2 H); $^{13}$C NMR ($CDCl_3$) $\delta$ 155.7, 154.7, 135.6, 135.4, 128.7, 128.2, 126.9, 111.0, 105.1, 71.4; MS (ES$^+$) $m/z$ 268.0 (M + Na)$^+$.

*2-(3-(Benzyloxy)-2-nitrophenoxy)-N,N-diethylethanamine (**6**).* A mixture of nitrophenol **5** (1.31 g, 5.4 mmol), 2-(diethylaminoethyl)-ethyl chloride hydrochloride (1.2 g, 7 mmol), $Cs_2CO_3$ (4.37 g, 13.4 mmol), and acetone (20 mL) was stirred at 50 °C for 3 h. The mixture was filtered and the filtrate was concentrated to a residue that was purified by flash silica gel chromatography, eluting with hexanes/ethyl acetate (5:1). Product fractions were pooled and concentrated to leave **6** (1.71 g, 93%) as a light yellow oil: $R_f$ = 0.22 ($CH_2Cl_2$/methanol, 95:5); $^1$H NMR ($CDCl_3$) $\delta$ 7.3 (m, 6 H), 6.62, (dd, $J_1$ = 3.6 Hz, $J_2$ = 14.1 Hz, 2 H), 5.16 (s, 2 H), 4.1 (t, $J$ = 10.5 Hz, 2 H), 2.8 (t, $J$ = 10.5 Hz, 2 H), 2.6 (q, $J$ = 11.9 Hz, 4 H), 1.0 (t, $J$ = 11.9 Hz, 6 H); $^{13}$C NMR ($CDCl_3$) $\delta$ 151.2, 150.8, 135.6, 130.9, 128.6, 128.2, 127.0, 105.9, 105.6, 70.9, 68.5, 51.2, 47.9, 11.9; MS (ES$^+$) $m/z$ 245.1 (M + H)$^+$.

*2-Amino-3-(2-(diethylamino)ethoxy)phenol (**7**).* 2-(Diethylamino)ethyl ether **6** (1.8 g, 5.2 mmol) was dissolved in 10% acetic acid in methanol (50 mL) in a 250 mL Parr hydrogenation bottle. Catalyst (20% $Pd(OH)_2$/C, 0.1 g) was added, and the mixture was hydrogenated at 40 psi of $H_2$ for ∼20 h. The reaction mixture was rapidly filtered over Celite, and the filtrate was concentrated and diluted with ethyl acetate. The solution was washed with 5% aqueous sodium carbonate, dried, and concentrated to a brown solid that was triturated in hot hexanes. The solids were collected and dried to leave **7** (0.95 g, 81%): mp 91−91.5 °C; $R_f$ = 0.21 ($CH_2Cl_2$/methanol, 85:15); $^1$H NMR ($CD_3OD$) $\delta$ 6.63 (t, $J$ = 8.2 Hz, 1 H), 6.51 (m, 2 H), 4.34 (t, $J$ = 5.1 Hz, 2 H), 3.60 (t, $J$ = 5.0 Hz, 2 H), 3.35 (m, 4 H), 1.37 (t, $J$ = 7.2 Hz, 6 H); $^{13}$C NMR ($CD_3OD$) $\delta$ 148.5, 147.9, 124.8, 120.1, 110.4, 105.4, 64.0, 52.7, 21.0, 9.2; MS (ES$^+$) $m/z$ 225.1 (M + H)$^+$.

*1-(Benzyloxy)-3-(4-bromobutoxy)-2-nitrobenzene (**8**).* To a mixture of DMF (5 mL), 1,4-dibromobutane (5 mL), and $Cs_2CO_3$ (1.66 g, 5.1 mmol) was added slowly a solution of nitrophenol **5** (0.5 g, 2.0 mmol) in DMF (5 mL). The mixture was stirred at room temperature for 16 h, and then DMF was removed in vacuo to leave an oil that was distributed between 1% aqueous HCl and ethyl acetate. The organic phase was dried and concentrated to a light yellow oil that was purified by flash silica gel chromatography, eluting with hexanes/ethyl acetate (6:1). Product fractions were pooled and concentrated to give **8** (0.702 g, 93%) as a light yellow oil: $R_f$ = 0.45 (hexanes/ethyl acetate, 2:1); $^1$H NMR ($CDCl_3$) $\delta$ 7.36 (m, 5 H), 7.26 (m, 1 H), 6.61 (m, 2 H), 5.16 (s, 2 H), 4.08 (t, $J$ = 5.8 Hz, 2 H), 3.46 (t, $J$ = 6.3 Hz, 2 H), 2.02 (m, 2 H), 1.92 (m, 2 H); $^{13}$C NMR ($CDCl_3$) $\delta$ 151.1, 150.9, 135.6, 131.0, 128.7, 128.2, 127.0, 106.1, 105.6, 70.9, 68.4, 33.4, 28.9, 27.5; MS (ES$^+$) $m/z$ 401.9, 403.9 (M + Na)$^+$.

*1-(2-(1H-Imidazol-1-yl)ethyl)-4-(4-(3-(benzyloxy)-2-nitrophenoxy)butyl)piperazine (**9a**).* A solution of bromobutyl ether **8** (1.0 g, 2.6 mmol), 1-[2-(1*H*-imidazol-1-yl)ethyl]piperazine (0.52 g,

2.9 mmol; Oakwood Products Inc.), *N*,*N*-diisopropylethylamine (5 mL), and acetonitrile (18 mL) was heated at reflux overnight. The solution was concentrated, and the residue was distributed between dichloromethane and 5% aqueous sodium carbonate. The organic phase was dried and concentrated to an orange oil that was purified by flash silica gel chromatography, eluting with dichloromethane: methanol/$NH_4OH$ (90:10:0.5). Product fractions was pooled and concentrated to leave **9a** (0.86 g, 68%) as an oil: $^1$H NMR ($CDCl_3$) $\delta$ 7.53 (s, 1 H), 7.36−7.22 (m, 6 H), 7.03 (s, 1 H), 6.97 (d, $J$ = 1.1 Hz, 1 H), 6.61 (m, 1 H), 5.15 (s, 1 H), 4.05 (t, $J$ = 6.3 Hz, 2 H), 4.01 (t, $J$ = 6.5 Hz, 2 H), 2.67 (t, $J$ = 6.5 Hz, 2 H), 2.48 (bs, 8 H), 2.36 (t, $J$ = 6.5 Hz, 2 H), 1.79 (m, 2 H), 1.61 (m, 2 H); $^{13}$C NMR ($CDCl_3$) $\delta$ 151.3, 150.8, 137.4, 135.6, 132.8, 130.9, 129.2, 128.7, 128.2, 127.0, 119.3, 105.8, 105.6, 70.9, 69.3, 58.6, 57.8, 53.3, 53.0, 44.7, 26.9, 23.1; MS ($ES^+$) $m/z$ 480.1 $(M + H)^+$.

*tert-Butyl 4-(4-(3-(Benzyloxy)-2-nitrophenoxy)butyl)piperazine-1-carboxylate (**9b**).* A solution of bromobutyl ether **8** (0.4 g, 1.05 mmol), 1-Boc-piperazine (0.282 g, 1.514 mmol) *N*,*N*-diisopropylethylamine (4 mL), and acetonitrile (10 mL) was heated at reflux for 12 h. The solution was concentrated and distributed between ethyl acetate and brine. The organic phase was dried and concentrated to residue that was purified by flash silica gel chromatography, eluting with ethyl acetate. Product fractions were pooled and concentrated to leave **9b** (0.505 g, 99%): $^1$H NMR ($CDCl_3$) $\delta$ 7.36 (m, 4H), 7.31 (m, 1 H), 7.24 (m, 1 H), 6.61 (m, 2 H), 5.16 (s, 2 H), 4.06 (t, $J$ = 6.2 Hz, 2 H), 3.41 (t, $J$ = 7.0 Hz, 4 H), 2.36 (t, $J$ = 7.0 Hz, 4 H), 1.80 (m, 2 H), 1.62 (m, 2 H), 1.46 (s, 9 H), 1.26 (t, $J$ = 7.2 Hz, 2 H); $^{13}$C NMR ($CDCl_3$) $\delta$ 154.9, 151.5, 150.9, 135.8, 131.0, 128.8, 128.3, 127.1, 106.0, 105.7, 79.7, 71.1, 69.4, 60.5, 58.1, 53.1, 28.6, 27.0, 23.2, 21.2, 14.3; MS ($ES^+$) $m/z$ 486.1 $(M + H)^+$.

*1-(4-(4-(3-(Benzyloxy)-2-nitrophenoxy)butyl)piperazin-1-yl)-2-(1H-imidazol-1-yl)ethanone (**10**).* Trifluoroacetic acid (2 mL) was added dropwise to a solution of **9b** (0.505 g, 1.04 mmol) in dichloromethane (8 mL), and the resultant mixture was stirred at room temperature for 3 h. The solution was concentrated to leave **9c** (0.52 g, quantitative) as the crystalline trifluoroacetate salt. This was then dissolved into DMF (10 mL) and *N*,*N*-diisopropylethylamine (3 mL), and the mixture was stirred at room temperature for 10 min followed by treatment with 1-ethyl-3-[3-dimethylaminopropyl]-carbodiimide hydrochloride (EDC·HCl, 0.22 g, 1.14 mmol), *N*-hydroxybenzotriazole (HOBt, 0.175 g, 1.14 mmol), and 2-(1*H*-imidazol-1-yl)acetic acid (0.197 g, 1.56 mmol; Tokyo Chemical Industry Co. Ltd.). After the mixture was stirred under $N_2$ for 16 h, DMF was removed in vacuo and the residue was distributed between dichloromethane and 5% aqueous sodium carbonate. The organic phase was dried and concentrated to an oil that was purified by flash silica gel chromatography, eluting with dichloromethane/methanol/$NH_4OH$ (95:5:0.5). Product fractions were pooled and concentrated to give **10** (0.37 g, 72%) as a yellow oil: $^1$H NMR ($CDCl_3$) $\delta$ 7.49 (s, 1 H), 7.36 (m, 5 H), 7.26 (m, 1 H), 7.09 (s, 1 H), 6.95 (s, 1 H), 6.61 (m, 1H), 5.16 (s, 2 H), 4.75 (s, 2 H), 4.07 (t, $J$ = 5.9 Hz, 2 H), 3.62 (m, 2 H), 3.44 (m, 2 H), 2.42 (t, $J$ = 4.9 Hz, 4 H), 2.39 (t, $J$ = 7.2 Hz, 2 H), 1.81 (m, 2 H), 1.62 (m, 2 H); $^{13}$C NMR ($CDCl_3$) $\delta$ 164.4, 151.3, 150.8, 138.0, 135.6, 131.0, 129.5, 128.7, 128.2, 127.0, 120.1, 105.9, 105.5, 70.9, 69.1, 57.6, 52.6, 47.9, 45.1, 42.3, 26.7, 22.9; MS ($ES^+$) $m/z$ 494.1 $(M + H)^+$.

*3-(4-(4-(2-(1H-Imidazol-1-yl)ethyl)piperazin-1-yl)butoxy)-2-aminophenol (**11a**).* Compound **9a** (0.86 g, 1.8 mmol) was dissolved in a mixture of 10% aqueous HCl (10 mL) and methanol (90 mL) in a Parr hydrogenation bottle. Catalyst (20% $Pd(OH)_2$/C, 0.05 g) was added, and the mixture was hydrogenated at 40 psi of $H_2$ for ∼40 h. The reaction mixture was rapidly filtered over Celite, and the filtrate was concentrated and diluted with ethyl acetate. The solution was washed with 5% aqueous sodium carbonate, dried, and concentrated to give **11a** (0.61 g, 95%) as a brown solid: $^1$H NMR ($CDCl_3$) $\delta$ 7.56 (s, 1 H), 7.05 (s, 1 H), 6.96 (s, 1 H), 6.52 (t, $J$ = 7.2 Hz, 1 H), 6.44 (s, 1 H), 6.37 (d, $J$ = 8.0 Hz, 1 H), 3.98 (m, 4 H), 2.66 (t, $J$ = 6.2 Hz, 2 H), 2.49 (bs, 8 H), 2.41 (t, $J$ = 6.5 Hz, 2 H), 1.78 1.68 (m, 2 H); $^{13}$C NMR ($CDCl_3$) $\delta$ 147.6, 145.5, 128.6, 124.9, 119.4, 117.3, 108.7, 103.7, 68.1, 58.4, 58.2, 53.0, 50.4, 44.7, 27.5, 23.3; MS ($ES^+$) $m/z$ 360.1 $(M + H)^+$.

*1-(4-(4-(2-Amino-3-hydroxyphenoxy)butyl)piperazin-1-yl)-2-(1H-imidazol-1-yl)ethanone (**11b**).* Compound **10** (0.37 g, 0.75 mmol) was dissolved in a mixture of 10% aqueous HCl (5 mL) and methanol (45 mL) in a Parr hydrogenation bottle. Catalyst (20% $Pd(OH)_2$/C, 0.02 g) was added, and the mixture was hydrogenated at 40 psi of $H_2$ for ∼40 h. Workup as described above for the synthesis of **11a** gave **11b** (0.27 g, 98%) as a brown solid: $^1$H NMR ($CD_3OD$) $\delta$ 7.78 (s, 1 H), 7.13 (s, 1 H), 7.06 (s, 1 H), 6.58 (m, 1 H), 6.43 (m, 2 H), 5.08 (s, 2 H), 4.03 (t, $J$ = 5.9 Hz, 2 H), 3.66 (s, 2 H), 3.62 (s, 2 H), 2.75 (s, 2 H), 2.65 (m, 4 H), 1.82 (m, 4 H); $^{13}$C NMR ($CD_3OD$) $\delta$ 174.8, 165.8, 148.0, 145.8, 138.1, 126.0, 123.0, 121.3, 118.2, 107.8, 103.5, 67.7, 57.3, 52.1, 51.8, 43.5, 40.9, 26.8, 22.2, 20.1; MS ($ES^+$) $m/z$ 374.1 $(M + H)^+$.

*Benzoxazinorifamycin (**2b**).* A mixture of aminophenol **7** (0.336 g, 1.5 mmol), rifamycin S (**12**, 2.085 g, 3 mmol), and 1,4-dioxane (20 mL) was stirred at room temperature overnight. The mixture was then concentrated to a black solid that was dissolved in 20 mL of methanol and treated with $MnO_2$ (0.3 g, 3.45 mmol). The mixture was stirred at room temperature for 30 min, filtered over Celite and the filtrate concentrated to a dark residue that was purified by flash silica gel chromatography, eluting with dichloromethane/methanol (95:5 to 90:10). Product fractions were pooled and concentrated to give partially purified **2b** as a deep purple solid. Further purification by preparative TLC was conducted on a 20 mg scale, eluting with dichloromethane/methanol (90:10). The yield was ∼55%: $R_f$ = 0.58 (dichloromethane/methanol, 85:15); HPLC $t_R$ = 9.4 min (98.1% purity). For $^1$H and $^{13}$C NMR ($CDCl_3$), see Supporting Information, Tables 1SI and 2SI. MS ($ES^+$) $m/z$ 900.1 $(M + H)^+$; HRMS (MALDI) calcd for $C_{49}H_{61}N_3O_{13}$ $[(M + H)^+]$, 900.4277; found 900.4269.

*Benzoxazinorifamycin (**2c**).* A mixture of aminophenol **11a** (80 mg, 0.22 mmol), rifamycin S (**12**, 220 mg, 0.32 mmol), and 1,2-dichloroethane (10 mL) was stirred at room temperature for 16 h. The reaction mixture was then concentrated to a black solid that was dissolved in 10 mL of methanol and treated with $MnO_2$ (80 mg, 0.92 mmol). The mixture was stirred at room temperature for 30 min, filtered over Celite, and concentrated to a dark residue that was purified by flash silica gel chromatography, eluting with dichloromethane/methanol/$NH_4OH$ (94:6:0.5). Product fractions were pooled and concentrated to give a solid that was further purified by preparative TLC, eluting with dichloromethane/methanol (92:8). The product band was processed to give **2c** (170 mg, 74%) as a dark purple solid: HPLC $t_R$ = 7.54 min (94.3% purity). For $^1$H and $^{13}$C NMR ($CDCl_3$), see Supporting Information, Tables 1SI and 2SI. MS ($ES^+$) $m/z$ 1035.1 $(M + H)^+$; HRMS (MALDI) calcd for $C_{49}H_{61}N_3O_{13}$ $[(M + H)^+]$, 1035.5074; found 1035.5095.

*Benzoxazinorifamycin (**2d**).* Reaction of a mixture of aminophenol **11b** (30 mg, 0.08 mmol), rifamycin S (**12**, 102 mg, 0.15 mmol), and 1,2-dichloroethane (4 mL) and subsequent purification were carried out exactly as described above for the synthesis of **2c** to provide **2d** (29 mg, 34.5%) as a dark purple solid: HPLC $t_R$ = 7.48 min (95.1% purity). For $^1$H and $^{13}$C NMR ($CDCl_3$), see Supporting Information, Tables 1SI and 2SI. MS ($ES^+$) $m/z$ 1049.2 $(M + H)^+$; HRMS (MALDI) calcd for $C_{49}H_{61}N_3O_{13}$ $[(M + H)^+]$, 1049.4866; found 1049.4857.

**Biological Materials and Methods.** *Expression and Purification of MTB RNAP (WT and RifR Mutants).* The wild-type MTB RNAP and the RifR mutants were prepared as previously described with minor alterations.[30] For cell lysis, the sonication method was preferred over the freeze/thaw method. For the remainder of the purification steps, the protocol outlined by Gill and Garcia[30] was followed.

*Cloning, Expression, and Purification of MTB SigA.* The pAvitag vector (modified pMSCG7 vector with an Avitag introduced between BglII and KpnI sites) was linearized with SspI at 37 °C for 1 h, and the reaction product was purified using the Qiagen PCR kit. The linearized pAvitag vector (1.6−2.0 $\mu$g) was treated with T4 DNA polymerase in 10× T4 polymerase buffer, 5 mM DTT, 4 mM dGTP in a final reaction volume of 60 $\mu$L. The mixture was incubated for 30 min at 22 °C and then for 20 min at 75 °C before being stored at −20 °C. PCR primers were designed to amplify the Rv2703/*sigA* gene encoding SigA from pSR01, which was provided by S. Rodrigue.[30] The primers

included an overhang sequence that complemented the vector ligation independent cloning (LIC) overhangs. The *sigA* gene was purified via Qiagen PCR kit. The purified PCR product (0.2 pmol) was incubated with T4 DNA polymerase, 5 mM DTT, 4 mM dCTP, and 10× T4 DNA polymerase in a final reaction volume of 20 μL. The mixture was incubated for 30 min at 22 °C and then for 20 min at 75 °C and stored at −20 °C. The treated *sigA* was incubated with treated pAvitag vector (∼0.2 pmol) for 10 min at 22 °C. Then 6.25 mM EDTA was added followed by incubation at 22 °C for 5 min before reducing the temperature to 4 °C. The annealed pAvitag vector containing *sigA* was transformed into BL21(DE3) CodonPlus RIPL cells.

For the expression of SigA protein in BL21(DE3) CodonPlus RIPL cells, the cells were grown in 500 mL of 2xTY liquid cultures containing 100 μg/mL carbenicillin and 30 μg/mL chloramphenicol at 37 °C with vigorous shaking until cell density reached $OD_{600\,nm}$ = 0.5−0.6. The protein was induced by the addition of isopropyl β-D-thiogalactoside (IPTG) to a final concentration of 1 mM. The cultures were allowed to incubate for an additional 20−24 h at 19 °C. The cells were harvested by centrifugation (6000*g*, 15 min, 4 °C). The cell pellet of each 500 mL culture was resuspended in 10 mL of $Ni^{2+}$-NTA bind buffer (300 mM NaCl, 50 mM $NaH_2PO_4$, 10 mM imidazole, pH 8.0). The freeze/thaw method was followed to lyse the cells, and it was repeated a total of three times. The sample was supplemented with 10 μL of Lysonase bioprocessing reagent and 100 μM phenylmethylsulfonyl fluoride (PMSF), and then the resulting lysate was cleared by centrifugation (21000*g*, 30 min, 4 °C). All further purification steps were performed at 4 °C. The lysate was incubated with 2 mL $Ni^{2+}$-NTA His·bind resin overnight with gentle shaking. Each supernatant−resin mixture was applied to individual columns. The columns were washed twice with 4 mL of $Ni^{2+}$-NTA wash buffer (300 mM NaCl, 50 mM $NaH_2PO_4$, 20 mM imidazole, pH 8.0), and the protein was then eluted in 6 mL of $Ni^{2+}$-NTA elute buffer (300 mM NaCl, 50 mM $NaH_2PO_4$, 250 mM imidazole, pH 8.0). The protein was concentrated to a final volume of ∼500 μL and then sterile-filtered with a 0.22 μm syringe before being applied to a HiPrep 16/60 Sephacryl S-200 HR (GE Healthcare) column, and the running buffer was RNAP storage buffer (10 mM Tris-HCl (pH 7.9), 0.1 mM EDTA, 0.1 mM DTT, 0.1 M NaCl). The fractions containing SigA were pooled together and concentrated to a final volume of ∼500 μL using Amicon centrifugal filter units (MWCO = 10 kDa). The enzyme was mixed with 1 volume of 100% glycerol and stored in liquid nitrogen. The final concentration of the enzyme was determined via Bradford assay using the Bio-Rad protein assay kit.

*In Vitro Transcriptional Activity of MTB RNAPs and Dose Response Curves.* Dose response studies with RLZ (**2a**) and analogues (**2b**−**d**) were performed via rolling circle transcription assay as described previously[30] to determine the $IC_{50}$ values. Each of the compounds was tested in duplicate ($n$ = 2). The concentration range used for the wild-type MTB RNAP (±SigA) was 1.56−100 nM for RLZ and analogues (**2b**−**d**). The concentration ranges used for MTB RNAP (D435V) with SigA were as follows: for **2a**, 39.1−2500 μM; for **2b**−**d**, 1.25−80 μM. The concentration ranges used for MTB RNAP (H445Y) with SigA were as follows: for **2a**, 20.5−5000 μM; for **2b**−**d**, 8.2−2000 μM. The concentration ranges used for MTB RNAP (S450L) with SigA were as follows: for **2a**, 8.2−2000 μM; for **2b**, 3.3−800 μM; for **2c** and **2d**, 1.64−400 μM. The final concentration of the wild-type MTB RNAP was 10 nM, whereas the final concentration of the mutant RNAPs was 100 nM in the reactions. The core RNAP and SigA were incubated for 30 min on ice in 1× RNAP reaction buffer (40 mM Tris-HCl (pH 8.0), 50 mM KCl, 10 mM $MgCl_2$, 0.01% Triton X-100) before adding the test compound and DNA nanocircle template (80 nM). Each reaction was initiated upon the addition of NTP solution (500 μM each NTP). The $IC_{50}$ values were determined via nonlinear regression to a modified four-parameter logistic equation as described previously.[30] The log($IC_{50}$) values and their standard errors (of the fit) are reported in Table 3SI (Supporting Information).

*MTB $MIC_{90}$ Assays.* All compounds were evaluated for $MIC_{90}$ vs MTB $H_{37}R_V$ using the microplate Alamar Blue assay (MABA) as previously described[32] except that 7H12 medium is now used (replacing 7H9 + glycerol + casitone + OADC). The use of this and other redox reagents such as MTT has shown excellent correlation with colony-forming unit (CFU) based and radiometric analyses of mycobacterial growth in many laboratories. The MIC is defined as the lowest concentration effecting a reduction in fluorescence (or luminescence) of 90% relative to controls. Isoniazid and rifampin are included as positive quality control compounds with expected MIC ranges of 0.025−0.1 and 0.06−0.125 μg/mL, respectively.

The low oxygen recovery (LORA) in vitro assay[33] is designed to detect compounds that may have the potential for shortening the duration of therapy through (more) efficient killing of the non-replicating persistor (NRP) population. The assay involves (1) adaptation of MTB to low oxygen through gradual, monitored, self-depletion of oxygen during culture in a sealed fermentor, (2) exposure for 10 days of the low-oxygen adapted culture to test compounds in microplates that are maintained under an anaerobic environment, thus precluding growth, and (3) subsequent evaluation of MTB viability as determined by the ability to recover. Recovery/viability is determined by either (a) (aerobic) subculture onto solid, drug-free mediim and determination of colony forming units or (b) the extent to which a luciferase-expressing strain can recover the ability to produce luminescence. Compounds such as isoniazid and ethambutol, which are considered to be devoid of "sterilizing activity", are inactive in this assay, while the rifamycins and the more potent fluoroquinolones, which do appear to eliminate some proportion of the persistor population and thus can affect treatment duration, are active, albeit at concentrations higher than the MICs for replicating cultures. Correlation between the CFU and luminescence readout has been good with the exception of the fluoroquinolone class for which luminescence underestimates absolute activity but not relative activity.

*Human Pregnane X Receptor (hPXR) Activation Assay.* To assess the ability of specific rifamycins to activate the human pregnane X receptor (hPXR), the hPXR activation assay system from Puracyp, Inc. was used. The manufacturer's protocol was followed for the 96-well plate assay. Briefly, the DPX2 cells were thawed in a 37 °C water bath and mixed thoroughly with culture medium. Then 100 μL of cell mixture was transferred into each well and the plate was incubated overnight in a 5% $CO_2$ incubator at 37 °C. The following day, the dosing medium was thawed in a 37 °C water bath. The dilutions of RLZ (**2a**) and analogues (**2b**−**d**) and RMP (**1a**, positive control) were prepared as described in the manual. The 96-well plate was removed from the incubator, and liquid from each well was discarded before adding 100 μL of the dilutions to the specific wells. Each dilution of the rifamycin derivative was tested in duplicate. The plate was placed in the 5% $CO_2$/37 °C incubator again for 24 h. The next day, the CellTiter-Fluor buffer and CellTiter-Fluor were thawed at room temperature before adding 5 μL of CellTiter-Fluor to 10 mL of CellTiter-Fluor buffer. The wells of the 96-well plate were emptied again, and 100 μL of CellTiter-Fluor reagent was added to each well. The plate was incubated for 1 h in the 5% $CO_2$/37 °C incubator. A Synergy H1 hybrid multimode microplate reader (BioTek) was used to measure fluorescence ($\lambda_{ex}$ = 390 nm; $\lambda_{em}$ = 505 nm). To obtain luminescence readings, the contents of ONE-Glo assay buffer were added to the ONE-Glo assay substrate, and then 100 μL of mixture was transferred into each well. The plate was read after 5 min where the luminometer was set for 5 s of preshake with 5 s/well read time. The relative luminescence units (RLUs) and relative fluorescence units (RFUs) were determined as outlined under the "Quantitation of PXR Receptor Activation" section of the manual. The normalized luciferase activity (RLU/RFU) was divided by the normalized DMSO control to represent the data as "fold activation" relative to the control. The replicate data points were averaged, and both the original data points and the average values were plotted as a function of log of concentration versus PXR activation. The average values were then fit by nonlinear regression to a modified four-parameter logistic equation using Kaleidagraph (Synergy Software, Essex, VT),

$$y = 1 + [(M3 - 1)/(1 + 10^{[(M1-M0)M2]})]$$

where M3 is the $EC_{MAX}$, 1 is the lower limit of the assay, M0 is the log of the rifamycin concentration, M1 is the log of the $EC_{50}$, and M2 is


dx.doi.org/10.1021/jm201716n | J. Med. Chem. 2012, 55, 3814−3826

the Hill slope. The data were normalized such that the lower limit was set to 1. M1, M2, and M3 were fit by the regression.

*Microsome Stability.* Test compound stock solutions were prepared at 200 μM in acetonitrile. An amount of 2 μL was added to 198 μL of PBS containing 1 mg/mL human or mouse microsome. After mixing, 25 μL aliquots were dispensed in triplicate in 96-well plates. Control and reaction wells received 25 μL of PBS and of 2 mM NADPH in PBS, respectively. Plates were incubated for 30 min at 37 °C with shaking at 600 rpm. Internal standard solution (150 μL) was added to each well to quench the reaction. For controls, quenching was done prior to incubation. Plates were centrifuged at 4000*g* for 30 min at 4 °C, and the supernatant was collected for analysis. The percentage of compound remaining and half-life of compound in microsomes were calculated according to the following formula:

$$\text{percentage remaining} = \frac{\text{reaction}}{\text{control}} \times 100$$

$$\text{half-life (min)} = -\frac{(\text{incubation time})[\ln(2)]}{\ln(\text{percentage remaining}/100)}$$

*Pharmacokinetics of Analogue* ***2b****.* Previously described methods were followed.[41,42]

*Single Dose Study.* Analogue **2b** was prepared in 0.5% CMC at 1 mg/mL. Healthy female BALB/c mice were administered 10 mg/kg suspension via oral gavage. Two mice per time point were used, and 0.4 mg/kg fentanyl was given 15 min prior to bleeding by intraperitoneal injection. For each mouse, at least 100 μL of venous blood was collected via retro-orbital bleeding in BD Vacutainer spray-coated K2EDTA tubes at 0.5, 1, 2, 4, 8, and 24 h postdose. Tubes were inverted several times and kept on ice. Blood was transferred to polypropylene tubes and centrifuged at 4000*g* for 30 min at 4 °C. The harvested plasma was transferred to new polypropylene tubes and stored at −80 °C until analysis. To each sample, 3× volume of chilled acetonitrile was added containing 0.2 μM internal standard (IS). The solution was vortexed and then subsequently centrifuged at 10000*g* for 15 min. Calibration standard samples were prepared by spiking the stock solution of analogue **2b** in acetonitrile into mouse plasma to yield the following concentrations: 0.097656, 0.195313, 0.390625, 0.78125, 1.5625, 3.125, 6.25, 12.5, 25, 50 μM. Supernatant was injected into an LC−MS/MS instrument for analysis. In addition, a blank (blank plasma extracted with 3× volume of IS) and a double blank (blank plasma extracted with 3× volume of pure acetonitrile) were prepared. The concentration of **2b** in blood sample for each time point was then determined.

*Multiple Dose Study.* Mice were dosed once daily for 5 consecutive days by oral gavage. Blood samples at time points 0.5, 1, 2, 4, 8, and 24 h were collected and analyzed in the same way as the single dose study. After collection of the blood, the mice were sacrificed by carbon dioxide asphyxiation. Lung tissue was aseptically removed, rinsed in 3 mL of PBS, air-dried on sterilized gauze pads, weighed, and suspended in 4× (solvent/tissue, w/v) PBS buffer. Lung tissue was homogenized, mixed, and extracted with 3× acetonitrile containing internal standard at 0.2 μM and centrifuged at 10000*g* for 15 min at 4 °C. The supernatant was collected for LC−MS/MS analysis. Calibration standard lung samples were prepared by spiking the stock solution of compound (in methanol or acetonitrile) into homogenized mouse lungs and extracting with 3× volume acetonitrile to yield the following concentrations: 0.024, 0.049, 0.098, 0.195, 0.39, 0.78, 1.56, 3.12, 6.25, 12.5, 25, 50 μM. In addition, a blank (blank lung tissue extracted with 3× volume of IS) and a double blank (blank lung tissue extracted with 3× volume of pure acetonitrile) were prepared. The concentration of **2b** in lung tissue for each time point was then determined.

## ■ ASSOCIATED CONTENT

### Ⓢ Supporting Information

Plots of **2a,c,d** with interaction surfaces of RNAP, stereoview of superimposed compounds **2a−d**, $^{1}$H and $^{13}$C NMR digital spectra of 2-aminoresorcinol ethers (**7**, **11a**, **11b**) and precursors, detailed digital data for benzoxazinorifamycins **2b−d** (1D and 2D NMR spectra along with $^{1}$H and $^{13}$C assignments and HRMS and HPLC traces), PK plots of analogue **2b** in plasma and lung tissue, table of log($IC_{50}$) values of **2a−d** against RNAP, and table of relative fluorescence units of **1a** and **2a−d** in the hPXR activation assay. This material is available free of charge via the Internet at http://pubs.acs.org.

## ■ AUTHOR INFORMATION


### Corresponding Author

*Phone: 734-764-5504. E-mail: showalh@umich.edu.

### Author Contributions

#These authors contributed equally.


### Notes

The authors declare no competing financial interest.

## ■ ACKNOWLEDGMENTS

We acknowledge generous support by the University of Michigan College of Pharmacy Ella and Hans Vahlteich and UpJohn Research Funds. We also acknowledge additional funding by the University of Michigan Office of the Vice President for Research and the Rackham Graduate School. We thank Dr. Paul Aristoff for stimulating discussions.

## ■ ABBREVIATIONS USED

RNAP, RNA polymerase; hPXR, human pregnane X receptor; SAR, structure−activity relationship; TB, tuberculosis; MTB, *Mycobacterium tuberculosis*; MDR-TB, multidrug-resistant tuberculosis; XDR-TB, extensively drug-resistant TB; Rif, rifamycin; RMP, rifampin; RFB, rifabutin; RLZ, rifalazil; PK, pharmacokinetic; RifR, rifamycin-resistant; MABA, microplate Alamar Blue assay; LORA, low oxygen recovery assay; MIC, minimum inhibitory concentration; RFB, rifabutin

## ■ REFERENCES


(1) *WHO Report 2008. Global Tuberculosis Control: Surveillance, Planning, Financing*; World Health Organization: Geneva, Switzerland, 2008.

(2) Barrera, L. The Basics of Clinical Bacteriology. In *Tuberculosis 2007: From Basic Science to Patient Care*; Palomino, J. C., Leão, S. C., Ritacco, V., Eds.; Amedeo Challenge, 2007; pp 93−112.

(3) Godreuil, S.; Tazi, L.; Bañuls, A.-L. Pulmonary Tuberculosis and Mycobacterium Tuberculosis: Modern Molecular Epidemiology and Perspectives. In *Encyclopedia of Infectious Diseases: Modern Methodologies*; Tibayrenc, M., Ed.; Wiley-Liss: Hoboken, NJ, 2007; pp 1−30.

(4) Garcia, A. B.; Palacios, J. J.; Ruiz, M. J.; Barluenga, J.; Aznar, F.; Cabal, M. P.; Garcia, J. M.; Diaz, N. Strong in vitro activities of two new rifabutin analogs against multidrug-resistant *Mycobacterium tuberculosis*. *Antimicrob. Agents Chemother.* **2010**, *54* (12), 5363−5365.

(5) Koul, A.; Arnoult, E.; Lounis, N.; Guillemont, J.; Andries, K. The challenge of new drug discovery for tuberculosis. *Nature* **2011**, *469* (7331), 483−490.

(6) (a) Siddiqi, M. I.; Kumar, A. Review of knowledge for rational design and identification of anti-tubercular compounds. *Expert Opin. Drug Discovery* **2009**, *4* (10), 1005−1015. (b) Lienhardt, C.; Vernon, A.; Raviglione, M. C. New drugs and new regimens for the treatment of tuberculosis: review of the drug development pipeline and implications for national programmes. *Curr. Opin. Pulm. Med.* **2010**, *16* (3), 186−193.

(7) Aristoff, P. A.; Garcia, G. A.; Kirchhoff, P. D.; Showalter, H. D. H. Rifamycins: obstacles and opportunities. *Tuberculosis* **2010**, *90* (2), 94−118.

(8) Saito, H.; Tomioka, H.; Sato, K.; Emori, M.; Yamane, T.; Yamashita, K.; Hosoe, K.; Hidaka, T. In vitro antimycobacterial activities of newly synthesized benzoxazinorifamycins. *Antimicrob. Agents Chemother.* **1991**, *35*, 542−547.

(9) (a) Lounis, N.; Roscigno, G. In vitro and in vivo activities of new rifamycin derivatives against mycobacterial infection. *Curr. Pharm. Des.* **2004**, *10*, 3229−3238. (b) Luna-Herrera, J.; Venkata Reddy, M.; Gangadharam, P. R. J. In vitro activity of the benzoxazinorifamycin KRM-1648 against drug-susceptible and multidrug-resistant tubercle bacilli. *Antimicrob. Agents Chemother.* **1996**, *39*, 440−444. (c) Tomioka, H. Current status of some antituberculosis drugs and the development of new antituberculous agents with special reference to their in vitro and in vivo antimicrobial activities. *Curr. Pharm. Des.* **2006**, *12*, 4047−4070.

(10) Yamamoto, T.; Amitani, R.; Suzuki, K.; Tanaka, E.; Murayama, T.; Kuze, F. In vitro bactericidal and in vivo therapeutic activities of a new rifamycin derivative, KRM-1648, against *Mycobacterium tuberculosis*. *Antimicrob. Agents Chemother.* **1996**, *40*, 426−428.

(11) (a) Moghazeh, S.; Pan, X.; Arain, T.; Stover, C. K.; Musser, J. M.; Kreiswirth, B. N. Comparative antimycobacterial activities of rifampin, rifapentine and KRM-1648 against a collection of rifampin-resistant *Mycobacterium tuberculosis* isolates with known rpoB mutations. *Antimicrob. Agents Chemother.* **1996**, *40*, 2655−2657. (b) Yang, B.; Koga, H.; Ohno, H.; Ogawa, K.; Fukuda, M.; Hirakata, Y.; Maesaki, S.; Tomono, K.; Tashiro, T.; Kohno, S. Relationship between antimycobacterial activities of rifampicin, rifabutin and KRM-1648 and rpoB mutations of *Mycobacterium tuberculosis*. *J. Antimicrob. Chemother.* **1998**, *42*, 621−628.

(12) (a) Mullin, S.; Rothstein, D. M.; Murphy, C. K. Activity of novel benzoxazinorifamycins against rifamycin-resistant *Streptococcus pyogenes*. *Antimicrob. Agents Chemother.* **2006**, *50*, 1908−1909. (b) Roblin, P. M.; Reznik, T.; Kutlin, A.; Hammerschlag, M. R. In vitro activities of rifamycin derivatives ABI-1648 (rifalazil, KRM-1648), ABI-1657, and ABI-1131 against *Chlamydia trachomatis* and recent clinical isolates of *Chlamydia pneumoniae*. *Antimicrob. Agents Chemother.* **2003**, *47*, 1135−1136.

(13) (a) Brooks, J. V.; Orme, I. M. Evaluation of once-weekly therapy for tuberculosis using isoniazid plus rifamycins in the mouse aerosol infection model. *Antimicrob. Agents Chemother.* **1998**, *42*, 3047−3048. (b) Klemens, S. P.; Grossi, M. A.; Cynamon, M. H. Activity of KRM-1648, a new benzoxazinorifamycin, against *Mycobacterium tuberculosis* in a murine model. *Antimicrob. Agents Chemother.* **1994**, *38*, 2245−2248.

(14) Kelly, B. P.; Furney, S. K.; Jessen, M. T.; Orme, I. M. Low-dose aerosol infection model for testing drugs for efficacy against *Mycobacterium tuberculosis*. *Antimicrob. Agents Chemother.* **1996**, *40*, 2809−2812.

(15) (a) Klemens, S. P.; Cynamon, M. H. Activity of KRM-1648 in combination with isoniazid against *Mycobacterium tuberculosis* in a murine model. *Antimicrob. Agents Chemother.* **1996**, *40*, 298−301. (b) Lenaerts, A. M.; Chase, S. E.; Cynamon, M. H. Evaluation of rifalazil in a combination treatment regimen as an alternative to isoniazid−rifampin therapy in a mouse tuberculosis model. *Antimicrob. Agents Chemother.* **2000**, *44*, 3167−3168. (c) Shoen, C. M.; Chase, S. E.; DeStefano, M. S.; Harpster, T. S.; Chmielewski, A. J.; Cynamon, M. H. Evaluation of rifalazil in long-term treatment regimens for tuberculosis in mice. *Antimicrob. Agents Chemother.* **2000**, *44*, 1458−1462.

(16) Rifalazil. *Tuberculosis (Edinburgh)* **2008**, *88*, 148−150.

(17) Mae, T.; Hosoe, K.; Yamamoto, T.; Hidaka, T.; Ohashi, T.; Kleeman, J. M.; Adams, P. E. Effect of a new rifamycin derivative, rifalazil, on liver microsomal enzyme induction in rat and dog. *Xenobiotica* **1998**, *28*, 759−766.

(18) Rose, L. M.; Porubek, D. J.; Montgomery, A. B. Method for Treatment of Bacterial Infections with Once- or Twice-Weekly Administered Rifalazil. WO2000035408A2, 2000.

(19) Dietze, R.; Teixeira, L.; Rocha, L. M. C.; Palaci, M.; Johnson, J. L.; Wells, C.; Rose, L.; Eisenach, K.; Ellner, J. J. Safety and bactericidal activity of rifalazil in patients with pulmonary tuberculosis. *Antimicrob. Agents Chemother.* **2001**, *45*, 1972−1976.

(20) (a) Rose, L. M.; Porubek, D. J.; Montgomery, A. B. Method for Treatment of Bacterial Infections with Once or Twice-Weekly Administered Rifalazil. US 6566354 B1, May 20, 2003. (b) Barry, P. J.; O'Connor, T. M. Novel agents in the management of *Mycobacterium tuberculosis* disease. *Curr. Med. Chem.* **2007**, *14* (18), 2000−2008.

(21) Portero, J.-L.; Rubio, M. New anti-tuberculosis therapies. *Expert Opin. Ther. Pat.* **2007**, *17*, 617−637.

(22) Artsimovitch, I.; Vassylyeva, M. N.; Svetlov, D.; Svetlov, V.; Perederina, A.; Igarashi, N.; Matsugaki, N.; Wakatsuki, S.; Tahirov, T. H.; Vassylyev, D. G. Allosteric modulation of the RNA polymerase catalytic reaction is an essential component of transcription control by rifamycins. *Cell* **2005**, *122* (3), 351−63.

(23) Sinz, M. W. Pregnane X receptor: prediction and attenuation of human CYP3A4 enzyme induction and drug−drug interactions. *Annu. Rep. Med. Chem.* **2008**, *43*, 405−418.

(24) Chrencik, J. E.; Orans, J.; Moore, L. B.; Xue, Y.; Peng, L.; Collins, J. L.; Wisely, G. B.; Lambert, M. H.; Kliewer, S. A.; Redinbo, M. R. Structural disorder in the complex of human pregnane X receptor and the macrolide antibiotic rifampicin. *Mol. Endocrinol.* **2005**, *19* (5), 1125−1134.

(25) Yamane, T.; Hashizume, T.; Yamashita, K.; Konishi, E.; Hosoe, K.; Hidaka, T.; Watanabe, K.; Kawaharada, H.; Yamamoto, T.; Kuze, F. Synthesis and biological activity of 3′-hydroxy-5′-aminobenzoxazinorifamycin derivatives. *Chem. Pharm. Bull. (Tokyo)* **1993**, *41* (1), 148−155.

(26) Dhingra, K.; Maier, M. E.; Beyerlein, M.; Angelovski, G.; Logothetis, N. K. Synthesis and characterization of a smart contrast agent sensitive to calcium. *Chem. Commun.* **2008**, *29*, 3444−3446.

(27) Binggeli, A.; Christ, A. D.; Green, L.; Guba, W.; Maerki, H. P.; Martin, R. E.; Mohr, P. Preparation of Benzoxazole, Oxazolopyridine, Benzothiazole and Thiazolopyridine Derivatives as Somatostatin Receptor Modulators and Antidiabetic Compounds. WO2007025897A2, 2007.

(28) Havera, H. J.; Strycker, W. G. 3-Substituted-5-phenyl-5-pyridylhydantoins. US3994904A, 1976.

(29) Mae, T.; Konishi, E.; Hosoe, K.; Hidaka, T. Isolation and identification of major metabolites of rifalazil in mouse and human. *Xenobiotica* **1999**, *29*, 1073−1087.

(30) Gill, S. K.; Garcia, G. A. Rifamycin inhibition of WT and Rif-resistant *Mycobacterium tuberculosis* and *Escherichia coli* RNA polymerases in vitro. *Tuberculosis* **2011**, *91* (5), 361−369.

(31) (a) Telenti, A.; Imboden, P.; Marchesi, F.; Lowrie, D.; Cole, S.; Colston, J.; Matter, L.; Schopfer, K.; Bodmer, T. Detection of rifampicin-resistance mutation in *Mycobacterium tuberculosis*. *Lancet* **1993**, *341*, 647−650. (b) Williams, D. L.; Spring, L.; Collins, L.; Miller, L. P.; Heifets, L. B.; Gangadharam, P. R. J.; Gillis, T. P. Contribution of rpoB mutations to development of rifamycin cross-resistance in *Mycobacterium tuberculosis*. *Antimicrob. Agents Chemother.* **1998**, *42*, 1853−1857.

(32) Collins, L.; Franzblau, S. Microplate Alamar Blue assay versus BACTEC 460 system for high-throughput screening of compounds against *Mycobacterium tuberculosis* and *Mycobacterium avium*. *Antimicrob. Agents Chemother.* **1997**, *41* (5), 1004−1009.

(33) Cho, S. H.; Warit, S.; Wan, B.; Hwang, C. H.; Pauli, G. F.; Franzblau, S. G. Low-oxygen-recovery assay for high-throughput screening of compounds against nonreplicating *Mycobacterium tuberculosis*. *Antimicrob. Agents Chemother.* **2007**, *51* (4), 1380−1385.

(34) Wang, J.; Huang, J.; Li, H.; Zhang, S. Synthesis of benzoxazinorifamycin derivatives and preliminary study of antibacterial activity. *Huaxi Yaoxue Zazhi* **2003**, *18* (4), 241−243.

(35) Labute, P. LowModeMD: implicit low mode velocity filtering applied to conformational search of macrocycles and protein loops. *J. Chem. Inf. Model.* **2010**, *50*, 792−800.

(36) *Molecular Operating Environment (MOE)*; Chemical Computing Group: Montreal, Canada, 2010.

(37) Watkins, R. E.; Wisely, G. B.; Moore, L. B.; Collins, J. L.; Lambert, M. H.; Williams, S. P.; Willson, T. M.; Kliewer, S. A.; Redinbo, M. R. The human nuclear xenobiotic receptor PXR: structural determinants of directed promiscuity. *Science* **2001**, *292* (5525), 2329−2333.

(38) Watkins, R. E.; Maglich, J. M.; Moore, L. B.; Wisely, G. B.; Noble, S. M.; Davis-Searles, P. R.; Lambert, M. H.; Kliewer, S. A.; Redinbo, M. R. 2.1 Å crystal structure of human PXR in complex with the St. John's wort compound hyperforin. *Biochemistry* **2003**, *42* (6), 1430−1438.
(39) Teotico, D. G.; Bischof, J. J.; Peng, L.; Kliewer, S. A.; Redinbo, M. R. Structural basis of human pregnane X receptor activation by the hops constituent colupulone. *Mol. Pharmacol.* **2008**, *74* (6), 1512−1520.
(40) Jacques, J.-F.; Rodrigue, S.; Brzezinski, R.; Gaudreau, L. A recombinant *Mycobacterium tuberculosis* in vitro transcription system. *FEMS Microbiol. Lett.* **2006**, *255*, 140−147.
(41) (a) Jayaram, R.; Gaonkar, S.; Kaur, P.; Suresh, B. L.; Mahesh, B. N.; Jayashree, R.; Nandi, V.; Bharat, S.; Shandil, R. K.; Kantharaj, E.; Balasubramanian, V. Pharmacokinetics−pharmacodynamics of rifampin in an aerosol infection model of tuberculosis. *Antimicrob. Agents Chemother.* **2003**, *47* (7), 2118−2124. (b) Jayaram, R.; Shandil, R. K.; Gaonkar, S.; Kaur, P.; Suresh, B. L.; Mahesh, B. N.; Jayashree, R.; Nandi, V.; Bharath, S.; Kantharaj, E.; Balasubramanian, V. Isoniazid pharmacokinetics−pharmacodynamics in an aerosol infection model of tuberculosis. *Antimicrob. Agents Chemother.* **2004**, *48* (8), 2951−2957.
(42) Shudo, J.; Pongpeerapat, A.; Wanawongthai, C.; Moribe, K.; Yamamoto, K. In vivo assessment of oral administration of probucol nanoparticles in rats. *Biol. Pharm. Bull.* **2008**, *31* (2), 321−325.